

ChemComm

Accepted Manuscript



This is an *Accepted Manuscript*, which has been through the Royal Society of Chemistry peer review process and has been accepted for publication.

Accepted Manuscripts are published online shortly after acceptance, before technical editing, formatting and proof reading. Using this free service, authors can make their results available to the community, in citable form, before we publish the edited article. We will replace this *Accepted Manuscript* with the edited and formatted *Advance Article* as soon as it is available.

You can find more information about *Accepted Manuscripts* in the [Information for Authors](#).

Please note that technical editing may introduce minor changes to the text and/or graphics, which may alter content. The journal's standard [Terms & Conditions](#) and the [Ethical guidelines](#) still apply. In no event shall the Royal Society of Chemistry be held responsible for any errors or omissions in this *Accepted Manuscript* or any consequences arising from the use of any information it contains.

Cite this: DOI: 10.1039/c0xx00000x

www.rsc.org/xxxxxx

ARTICLE TYPE

Hierarchical Bi₂MoO₆ Nanosheet-Built Frameworks with Excellent Photocatalytic Properties

Ying Ma^{a,b}, Yulong Jia^{a,b}, Zhengbo Jiao,^a Min Yang^a, Yanxing Qi^{a,*} and Yingpu Bi^{a,*}

Received (in XXX, XXX) Xth XXXXXXXXX 20XX, Accepted Xth XXXXXXXXX 20XX

DOI: 10.1039/b000000x

Herein, we demonstrate for the first time the fabrication of one-dimensional (1D) Bi₂MoO₆ inter-crossed nanosheet-built frameworks by using MoO₃ nanobelts as the growth templates and molybdate source. Especially, this novel Bi₂MoO₆ framework structure exhibits remarkably enhanced photocatalytic activity toward the degradation of organic dyes under visible-light irradiation, far exceeding that of conventional Bi₂MoO₆ nanoplates and nanoparticles. The photoelectrochemical study suggests that the hierarchical framework structure could facilitate the photoinduced charge separation and transfer from the inter-crossed Bi₂MoO₆ nanosheets, which may make a significant contribution to the enhanced photocatalytic activity.

Semiconductor photocatalysts have attracted considerable attention over the past decades due to their potential applications for solving current energy and environmental issues by utilizing the abundant solar energy. Up to now, various semiconductors, especially TiO₂¹⁻³ and ZnO⁴⁻⁷, have been extensively studied and proven to be powerful catalysts for diverse photo-chemical reactions, such as splitting water into hydrogen, degradation of organic waste, and artificial photosynthesis, etc. However, it should be noted that limited by large band gap (3.2 eV), these photocatalysts can only absorb the ultraviolet light ($\lambda \leq 400$ nm), which greatly restricts their efficiencies for the utilization of solar energy. To address this issue, much effort has been devoted to the exploration and fabrication of novel semiconductor materials with appropriate band-gap for improving the photocatalytic performances. Among them, Bi₂MoO₆ has recently become a popular target owing to its typical E_g (2.6 eV) and the excellent utilization of visible-light absorption. More specifically, as an important aurivillius oxide possessing the perovskite-like layered structure, Bi₂MoO₆ plate-like structures could be more easily obtained, which could effectively enhance the photocatalytic properties as a result of the increased active sites.⁸ More recently, the Bi₂MoO₆ nanosheet-built hierarchical structures, including nanofibers^{9,10}, hollow spheres^{11,12}, and flower-like structures¹³, have been extensively reported, and their photocatalytic behaviours could be further improved. However, note that the previous work mostly focused on the building hierarchical structures with densely packed Bi₂MoO₆ nanosheets. Up to now, the rational design, fabrication, and photocatalytic study of hierarchical architectures consisted of inter-crossed Bi₂MoO₆

nanosheets have been rarely reported.

Herein, we demonstrate for the first time the controlled fabrication of 1D Bi₂MoO₆ nanosheet-built frameworks (HBNF) structure with uniform nanochannels by simple hydration treatment of MoO₃ nanobelts, in which, MoO₃ nanobelts serve as both growth templates and molybdate source. Furthermore, it has been found that Bi₂MoO₆ nanosheet-built frameworks exhibit much higher photocatalytic performance than conventional Bi₂MoO₆ nanoplates and nanoparticles for the degradation of organic contaminations under visible light irradiation. Furthermore, these demonstrations clearly reveal that the controlled fabrication of hierarchical inter-crossed frameworks could serve as an alternative strategy for further improving the photocatalytic performance.

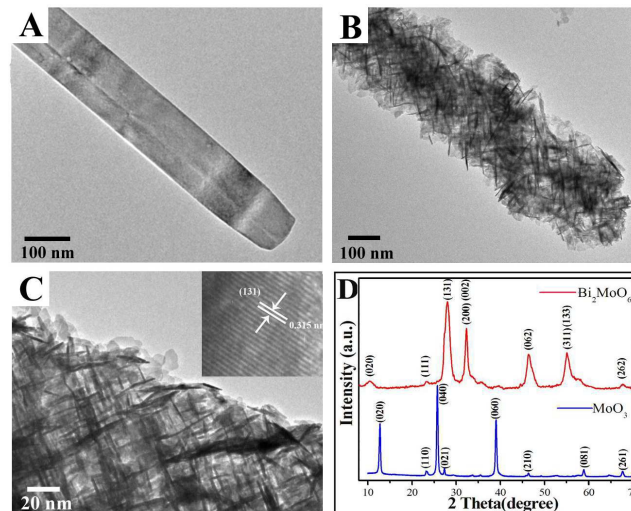


Fig. 1 The TEM images of (A) MoO₃ nanobelts, (B) and (C) Bi₂MoO₆ nanosheet-built framework (HBNF) (inset: the HRTEM image of HBNF), (D) XRD pattern of the precursor and product.

Fig. 1A show the typical transmission electron microscope (TEM) image of single-crystalline MoO₃ nanobelts synthesized through a modified hydrothermal method¹⁴, which would serve as the growth templates for the subsequent fabrication of 1D Bi₂MoO₆ nanosheet-built frameworks. It can be clearly seen from both TEM and SEM images (shown in Fig. S1, Fig S5A) that the as-prepared MoO₃ nanobelts possess rectangular cross-sections with an average width of ~ 120 nm and a length of about tens

micrometers. More specifically, it is confirmed that the MoO_3 grow along the [001] direction and two sets of crystal lattice fringes correspond to the {100} and {001} atomic spacings. Interestingly, when these MoO_3 nanobelts reacted with $\text{Bi}(\text{NO}_3)_3$ in aqueous solutions at 120°C , the hydrolysis reaction process of MoO_3 into MoO_6^{2-} ions occurred immediately, which would react with Bi^{3+} ions to form Bi_2MoO_6 hierarchical architectures (Fig. S3). The TEM image of Bi_2MoO_6 nanoproductions has been shown in Fig. 1B and S2, clearly indicating that a novel framework structure with an average diameter of 200 nm has been obtained by this simple reflux process. More specifically, the enlarged TEM image (Fig. 1C) clearly reveals that this framework structure is constructed by numerous inter-crossed ultra-thin nanosheets with an average thickness of 6 nm (inset of Fig. S2B). The corresponding high resolution TEM (HRTEM) image of the nanosheet building block (inset of Fig. 1C) demonstrates that the planar spacing is measured to be 0.315 nm, corresponding to the (131) crystal planes of orthorhombic Bi_2MoO_6 , indicating that these nanosheets grow vertically (131) facet and aggregate into a framework structure.¹¹

Furthermore, the X-ray diffraction (XRD) patterns (Fig. 1D) clearly reveal that the diffraction peaks of MoO_3 nanobelts can be indexed to the orthorhombic structure of $\alpha\text{-MoO}_3$ (JCPDS No.05-0508). However, after the heating treatment, all the diffraction peaks of nanosheet-built frameworks could be indexed to the orthorhombic structure of $\gamma\text{-Bi}_2\text{MoO}_6$ (JCPDS. No. 21-0102), and no any diffraction peak of MoO_3 has been observed. Moreover, the X-ray photoelectron spectroscopy (XPS) has also been performed to investigate the surface composition as well as valence state of Bi_2MoO_6 nanosheet-built frameworks. As shown in Fig. S4, all the peaks correspond to Bi, Mo, O and C elements (in which the C element was used to calibration) can be clearly detected and their valence states are consistent with the corresponding standardized binding energies. The above demonstrations clearly reveal that the MoO_3 nanobelts could be successfully and completely transformed into 1D Bi_2MoO_6 nanosheet-built frameworks through this simple template growth process.

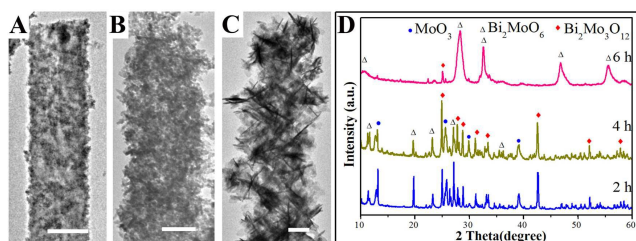
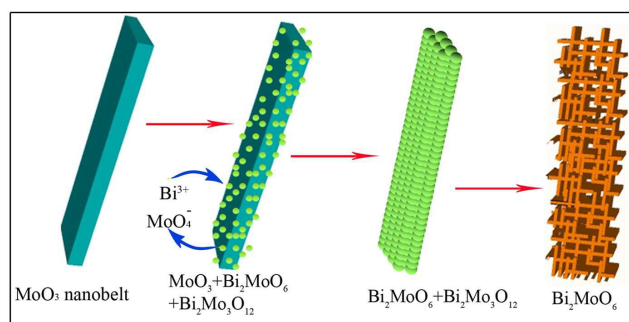


Fig. 2 TEM images of samples reacted for (A) 2 h, (B) 4 h, (C) 6 h and (D) the corresponding XRD pattern. (the scale bar in the TEM images represent 100 nm)

Furthermore, the morphological evolutions of intermediate products at different reaction time have been studied detailed to address of the possible growth process of Bi_2MoO_6 frameworks (Fig. 2, Fig S5). The TEM image shown in Fig. 2A clearly reveal that when the MoO_3 nanobelt precursors reacted with $\text{Bi}(\text{NO}_3)_3$ aqueous solution for 2 h, the surface of MoO_3 nanobelts have been completely covered by small nanoparticles, and the colour of reaction solution transformed gradually from white to yellow.

However, further increasing the reaction time up to 4 h, the regular rectangular nanobelts have been completely transformed into 1D disordered nanostructure consisted of numerous small particles. At 6 h, these nanoparticles have grown into nanosheets and a novel tree-like nanostructure has been formed (shown in Fig. 2C). Finally, Bi_2MoO_6 nanosheet-built frameworks with a uniform and perfect structure evolved as a result of the Ostwald ripening process (Fig. 1B). Furthermore, the evolution of composition and crystalline structure of these intermediate products during the growth process have been clarified (Fig. 2D). It is obviously that except for MoO_3 , the diffraction peaks of both Bi_2MoO_6 and $\text{Bi}_2\text{Mo}_3\text{O}_{12}$ could be observed obviously at 2 h, indicating that the formed hetero-particles on MoO_3 nanobelts could be attributed to the composite of Bi_2MoO_6 and $\text{Bi}_2\text{Mo}_3\text{O}_{12}$. When the hydrothermal reaction was carried out for 4 h, the diffraction peaks of MoO_3 were gradually reduced, and the peaks of Bi_2MoO_6 and $\text{Bi}_2\text{Mo}_3\text{O}_{12}$ were significantly enhanced. At 6 h, the diffraction peaks of MoO_3 have completely disappeared, and the main peaks could be indexed to Bi_2MoO_6 . Moreover, some small diffraction peaks corresponding to $\text{Bi}_2\text{Mo}_3\text{O}_{12}$ could also be detected. Finally, the novel nanosheet-built framework structure consisted of pure orthorhombic Bi_2MoO_6 crystal has been obtained at 8 h.



Scheme 1 Schematic representation of the synthesis of hierarchical Bi_2MoO_6 nanosheet-built framework through the anion-exchange reaction of the MoO_3 nanobelt with Bi^{3+} anion at controlled conditions.

On the basis of these results, we proposed a possible growth process for the transformation of MoO_3 nanobelts into HBNF under the present synthetic condition, which was illustrated in Scheme 1. It is well established that the MoO_3 crystals in water can be gradually hydrated to form H_2MoO_4 (eq 1). Thereby, the formed H_2MoO_4 molecules on the surface of MoO_3 nanobelts could directly react with Bi^{3+} anions to form Bi_2MoO_6 (eq 2) and $\text{Bi}_2\text{Mo}_3\text{O}_{12}$ (eq 3) nanoparticles *via* ion-exchange process, respectively. With increasing the reaction time, the MoO_3 nanobelts have been completely hydrated and transformed into Bi_2MoO_6 and $\text{Bi}_2\text{Mo}_3\text{O}_{12}$ nanoparticles with an incompact 1D structure. Under the heating conditions, the $\text{Bi}_2\text{Mo}_3\text{O}_{12}$ gradually converted into Bi_2MoO_6 nanosheets (eq 4).^{15,16} Moreover, during the transform process, the anisotropic growth of Bi_2MoO_6 nanosheets make them interconnection with each other. Finally, when the $\text{Bi}_2\text{Mo}_3\text{O}_{12}$ has completely transformed into Bi_2MoO_6 , kinetically stable Bi_2MoO_6 nanosheet-built framework has been fabricated. However, the exact growth mechanism of Bi_2MoO_6 frameworks can not be completely understood and a more detailed study is still underway.

- (1) $\text{MoO}_3 + \text{H}_2\text{O} \rightarrow \text{H}_2\text{MoO}_4$
- (2) $\text{H}_2\text{MoO}_4 + 2\text{Bi}(\text{NO}_3)_3 \cdot 5\text{H}_2\text{O} \rightarrow \text{Bi}_2\text{MoO}_6 + 6\text{HNO}_3 + 8\text{H}_2\text{O}$
- (3) $3\text{H}_2\text{MoO}_4 + 2\text{Bi}(\text{NO}_3)_3 \cdot 5\text{H}_2\text{O} \rightarrow \text{Bi}_2\text{Mo}_3\text{O}_{12} + 6\text{HNO}_3 + 10\text{H}_2\text{O}$
- (4) $\text{Bi}_2\text{Mo}_3\text{O}_{12} \rightarrow \text{Bi}_2\text{MoO}_6 + 2\text{MoO}_3$

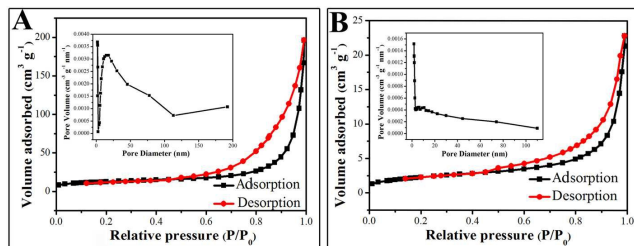


Fig. 3 Nitrogen adsorption-desorption isotherms measured at 76 K from obtained HBNF (A) and BMNS (B). Insets: the pore size distribution of the corresponding crystals.

To further study the surface area and nanochannels in the as-fabricated HBNF, the Brunauer–Emmett–Teller (BET) nitrogen adsorption isotherm experiments have been performed and results have been shown in Fig. 3A. Moreover, the related experiments on the BMNS have also been measured for comparison (Fig. 3B). It can be clearly observed that the nitrogen adsorption-desorption isotherms on HBNF and BMNS could be both identified as type IV, revealing the existence of abundant mesoporous structures in these two samples.¹⁷ More specifically, the as-prepared HBNF possess a larger adsorption volume and specific surface area (44.64 m²/g) than that of BMNS sample (8.40 m²/g). Furthermore, the distribution of nanochannels and pores in these two samples have also been studied and shown in the inset of Fig. 3. It can be clearly seen from Fig. 3A that the main pore size distribution of HBNF is generally in the range of 15–20 nm, which may be generated as a result of the inter-crossed nanosheets. However, in the case of BMNS, no primary pore size distribution has been observed due to their pure sheet-like structure (inset image of Fig. 3B). These demonstrations clearly reveal that the rational assembly of Bi₂MoO₆ nanosheets into inter-crossed frameworks could not only greatly increase the specific surface area, but also form the nanopores as well as nanochannels.

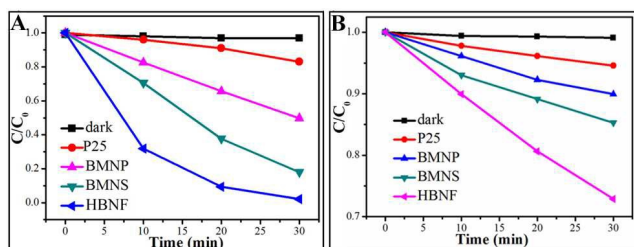
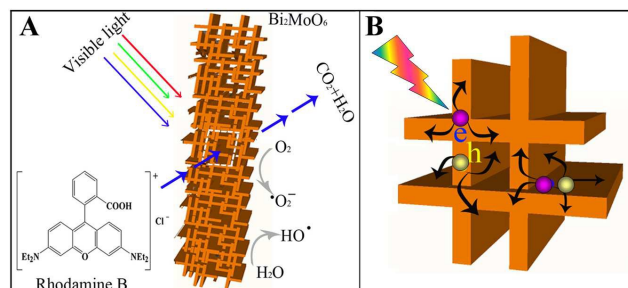


Fig. 4 The degradation curves of RhB (A) and phenol (B) over different photocatalysts under visible-light irradiation.

Their photocatalytic behaviours were explored for the degradation of Rhodamine B (RhB) dyes under visible-light irradiation (Fig. S6). To the best of our knowledge, this novel Bi₂MoO₆ nanosheet-built framework structure was used, for the first time, as the catalyst for these photocatalytic reactions. For comparison, the photocatalytic performances of Bi₂MoO₆ nanosheets, nanoparticles, and Degussa-P25, have also been studied and compared in Fig. 4A, Fig. S7, and Fig. S8A. It can be clearly seen that except for Degussa-P25¹⁸, all the Bi₂MoO₆

photocatalysts exhibit excellent photocatalytic activities for the RhB degradation. Among them, the Bi₂MoO₆ nanosheet-built framework structure exhibits the highest photocatalytic activity, which can completely degrade RhB dye in only 30 min. Furthermore, the degradation efficiency of RhB dye over Bi₂MoO₆ nanosheet is about 80%, while only 35% of RhB dye can be degraded over the Bi₂MoO₆ nanoparticles. Moreover, the photocatalytic behaviours for the degradation of colorless phenol under visible-light irradiation have also been explored. It can be clearly seen from Fig. 4B and Fig. S8B that Bi₂MoO₆ nanosheet-built frameworks still exhibit the highest photocatalytic activity for phenol degradation, which is consistent with the experimental results of RhB degradation. Thereby, it can be concluded that the enhanced performance of Bi₂MoO₆ frameworks could be ascribed to their specific hierarchical nanosheet-built structure, large surface area and nanochannels, which could provide more active sites and thus facilitate diffuse of reactants and products during the photocatalytic reaction. Fig. S9 shows the transient photocurrent responses of the samples under intermittent 300W Xe lamp irradiation. It can be seen that the Bi₂MoO₆ nanosheet-built framework exhibit much higher photocurrent intensity than Bi₂MoO₆ nanosheets and nanoparticles, indicating the more efficient photoinduced charge separation and transfer in hierarchical Bi₂MoO₆ nanosheet-built framework, which is in good agreement with the above photocatalytic activities. On the basis of the above results, it can be confirmed that the photocatalytic and photoelectric performances of Bi₂MoO₆ semiconductor can be further optimized by the construction of inter-crossed nanosheet-built framework structures.



Scheme 2 Schematic illustration (A and B) of photodegradation of RhB by HBNF.

On the basis of above results, we identified some possible reasons to clarify the higher photocatalytic activity of HBNF structure than both Bi₂MoO₆ nanosheets and nanoparticles. As shown in Scheme 2A, the frameworks could effectively enhance the visible light absorption as a result of their unique inter-crossed structures and large specific surface area compared with nanosheets and nanoparticles. Moreover, the nanochannels in the range of 15–20 nm could facilitate the rapid transfer of organic molecule from both exterior and inner of framework, which can greatly increase the active sites.^{19,20} More importantly, as shown in Scheme 2B, the nanosheet-built framework could facilitate the hole and electron rapid transfer from different orientation under visible light irradiation as a result of their unique inter-crossed nanosheets, which could greatly promote the effective separation of photoexcited electron–hole pairs and decrease the probability of electron–hole recombination confirmed by photoelectric results.

In summary, we have developed a facile and rapid process for fabricating 1D Bi₂MoO₆ nanosheet-built framework structures by simply reacting MoO₃ nanobelts with Bi(NO₃)₃ aqueous solution with a reflux process. Moreover, these Bi₂MoO₆ nanosheet-built frameworks exhibit much higher visible-light-driven photocatalytic activity and photoelectric property than Bi₂MoO₆ nanosheets and nanoparticles. More importantly, the rational fabrication of hierarchical nanosheet-built framework may be an effective technique for development of highly efficient visible-light sensitive photocatalysts. The extension of this simple self-template strategy for the transformation of MoO₃ nanobelts to the synthesis of other hierarchical framework structures is under way in our research group.

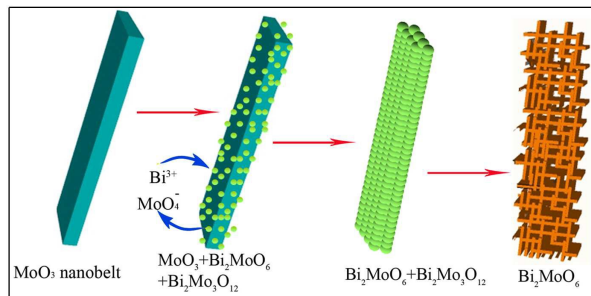
Notes and references

- ¹⁵ ^a State Key Laboratory for Oxo Synthesis & Selective Oxidation, and National Engineering Research Center for Fine Petrochemical Intermediates, Lanzhou Institute of Chemical Physics, CAS, Lanzhou 730000, China. E-mail: yingpubi@licp.cas.cn; qiyx@lzb.ac.cn
- ¹⁶ ^b University of Chinese Academy of Sciences, Beijing 100049, China.
- ²⁰ † Electronic Supplementary Information (ESI) available: Experimental section, additional figures and discussions. See DOI: 10.1039/b000000x/
1. T.R. Gordon, M. Cargnello, T.J. Paik, *J. Am. Chem. Soc.*, 2012, **134**, 6751–6761.
 2. J.S. Chen, Y.L. Tan, C.M. Li, Y.L. Cheah, D.Y. Luan and X.W. Lou, *J. Am. Chem. Soc.*, 2010, **132**, 6124–6130.
 3. W. Ho, J.C. Yu, S. Lee, *Chem. Comm.*, 2006, **10**, 1115–1117.
 4. F. Xu, P. Zhang, A. Navrotsky, Z.Y. Yuan, T.Z. Ren, M. Halasa and B.L. Su, *Chem. Mater.*, 2007, **19**, 5680–5685.
 5. H.B. Lu, S.M. Wang, L. Zhang, *J. Mater. Chem.*, 2011, **21**, 4228–4234.
 6. X. Wang, M.Y. Liao, Y.T. Zhong, *Adv. Mater.*, 2012, **24**, 3421–3425.
 7. C.G. Tian, Q. Zhang, A.P. Wu, *Chem. Comm.*, 2012, **48**, 2858–2860.
 8. J.L. Long, S.C. Wang, H.J. Chang, *Small*, 2014, **10**, 2791–2795.
 9. M.Y. Zhang, C.L. Shao, J.B. Mu, X.M. Huang, *J. Mater. Chem.*, 2012, **22**, 577–584.
 10. M.Y. Zhang, C.L. Shao, J.B. Mu, Z.Y. Zhang, *CrystEngComm*, 2012, **14**, 605–612.
 11. G.H. Tian, Y.J. Chen, W. Zhou, K. Pan, *J. Mater. Chem.*, 2011, **21**, 887–892.
 12. C.S. Guo, J. Xu, S.F. Wang, *CrystEngComm*, 2012, **14**, 3602–3608.
 13. Z.Q. Li, X.T. Chen, Z.L. Xue, *CrystEngComm*, 2013, **15**, 498–508.
 14. L. Zhou, L.C. Yang, P. Yuan, *J. Phys. Chem. C*, 2010, **114**, 21868–21872.
 15. M.B. Andrew, S. Gopinathan, *Chem. Mater.*, 2003, **15**, 146–153.
 16. L.D. Krenzke, G.W. Keulks, *J. Catal.*, 1980, **64**, 295–302.
 17. D.H. Chen, F.Z. Huang, Y.B. Cheng and R.A. Caruso, *Adv. Mater.*, 2009, **21**, 1–5.
 18. D.C. Hurum, A.G. Agrios, K.A. Gray, *J. Phys. Chem. B*, 2003, **107**, 4545–4549.
 19. H.K. Wang, A.L. Rogach, *Chem. Mater.*, 2014, **26**, 123–133.
 20. R. Schreiber, J. Do, E.M. Roller, *Nat. Nanotechnol.*, 2014, **9**, 74–78.

55

Hierarchical Bi_2MoO_6 Nanosheet-Built Frameworks with Excellent Photocatalytic Properties

Ying Ma, Yulong Jia, Zhengbo Jiao, Min Yang, Yanxing Qi*, and Yingpu Bi*



We demonstrate a simple and effective strategy for rationally fabricating one-dimensional (1D) Bi_2MoO_6 nanosheet-built frameworks, which exhibit much higher photocatalytic performances than conventional Bi_2MoO_6 nanoplates and nanoparticles for the degradation of organic contaminations under visible light irradiation.